Supplementary Information

Side-binding proteins modulate actin filament dynamics

Alvaro H. Crevenna[1,2]*, Marcelino Arciniega[3,4], Aurélie Dupont[1,6] , Kaja Kowalska[2], Oliver F. Lange[4,5,7], Roland Wedlich-Söldner[2,9] and Don C. Lamb[1,6,8]

[1] Physical Chemistry, Department for Chemistry and Biochemistry and Center for Nanoscience (CeNS), Ludwig-Maximilians-Universität München, Butenandtstraße 5-13, Haus E, 81377, München, Germany.

[2] Cellular Dynamics and Cell Patterning, Max Planck Institute of Biochemistry, Am Klopferspitz 18, 82152, Martinsried, Germany.

[3] Max Planck Institute of Biochemistry, Am Klopferspitz 18, 82152, Martinsried, Germany.

[4] Department Chemie, Technische Universität München, Lichtenbergstraße 4, 85748 Garching, Germany.

[5] Biomolecular NMR and Munich Center for Integrated Protein Science, Technische Universität München, Lichtenbergstraße 4, 85748 Garching, Germany.

[6] Munich Center for Integrated Protein Science (CiPSM), Ludwig-Maximilians-Universität München, Butenandtstraße 11, 81377 München, Germany.

[7] Institute of Structural Biology, Helmholtz Zentrum München, 85764 Neuherberg, Germany.

[8] Department of Physics, University of Illinois at Urbana-Champaign, 1110 West Green Street, Urbana, IL 61801, USA.

[9] Present address: Institute of Cell Dynamics and Imaging, Von-Esmarch-Straße 56, 48149, Münster, Germany.

* Correspondence: alvaro.crevenna@cup.uni-muenchen.de

Table of contents **Page**

Table S1. Results of a Monte Carlo Simulation describing the affect of lattice protein binding to the association rate of actin monomer binding to filaments.

The binding of an actin-binding protein onto the lattice of a filament leads to changes (with magnitude α) in association kinetics that are propagated over a certain characteristic length L_C, as a number of monomers.

	α	L_C (monomers)
VASP	9[a] (7-10)[b]	160 (145-175)
α-actinin	0.4 (0.4-0.7)	1 (1-11)
Filamin	0.4 (0.2-0.8)	11 (1-101)
NEM-myosin	0.7 (0.3-0.9)	11 (1-201)

[a] The value obtained by minimizing the χ^2.

[b] The values in parenthesis represent the 68% confidence interval.

Table S2. Filament and monomer actin models used for Brownian Dynamics simulations

Actin	Model name	PDB ID	Tecnique	Reference
filament	Narita	2Y83	Cryo-EM[a]	(Narita et al., 2011)
filament	Murakami	3G37	Cryo-EM[a]	(Murakami et al., 2010)
filament	Galkin	3J0S	Cryo-EM[a]	(Galkin et al., 2011)
filament	Oda	2ZWH	FD[b]	(Narita et al., 2009)
filament	Namba	3MFP	Cryo-EM[a]	(Fujii et al., 2010)
filament	Holmes ‘90	1ATN	X-ray diffracion[c]	(Holmes et al., 1990)
filament	Homes ‘10	1J6Z	X-ray diffracion[c]	(Splettstoesser et al., 2011)
filament	Behrmann	4A7N	Cryo-EM[a]	(Behrmann et al., 2012)
filament	Modes1-5	Author data	Cryo-EM[a]	(Galkin et al., 2010)
monomer	Profilin	2BTF	X-ray diffracion	(Schutt et al., 1993)
monomer	ATP-actin	1ATN	X-ray diffracion	(Kabsch et al., 1990)
monomer	ADP-actin	1J6Z	X-ray diffracion	(Otterbein et al., 2001)

[a] Electron Microscopy.
[b] Fiber Diffraction.
[c] Filament model was built, using the PDB of the monomer and based on the reported rotation matrix.

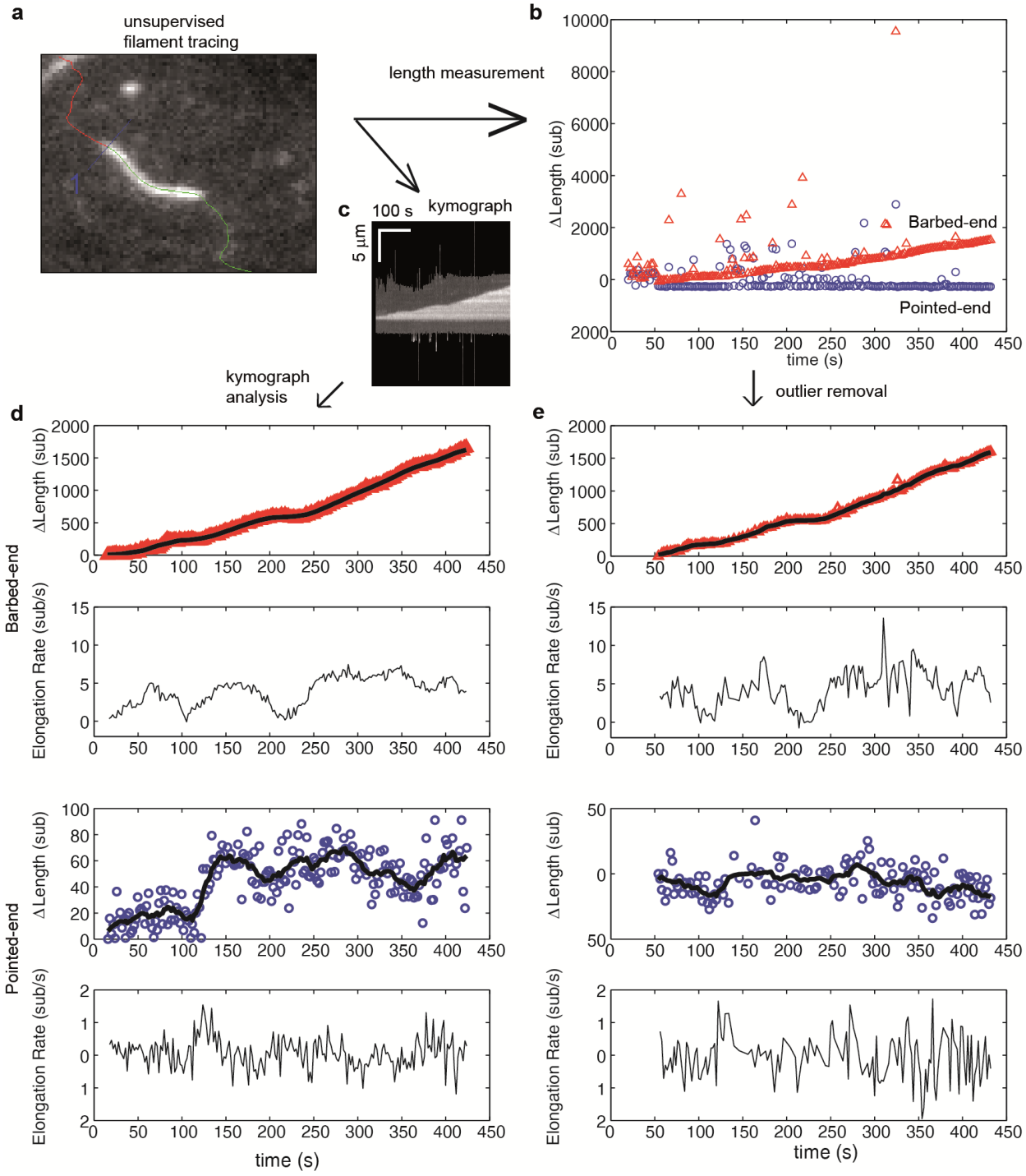

Figure S1. Comparison of algorithms for end-detection and filament growth. (**a**) An image from a TIRF measurement of the elongation of an actin filament tethered to the surface using filamin. From the movie, an unsupervised filament tracing analysis, developed by Kuhn and Pollard (Kuhn and Pollard, 2005), provides: (**b**) an estimate of the length of the filament based upon the algorithm; and (**c**) a kymograph of filament growth is produced. (**d**) From the

kymograph, we determine the position of the ends of the filament using an error function fit as implemented by (Demchouk et al., 2011), which generates a reliable estimate of position of the filament ends. The growth of the ends and the elongation rate, determined from the consecutive differences in the position, are shown for the pointed and barbed ends. Points represent raw data of the change in length, ΔL, as a function of time while the black solid lines correspond to the data using a running mean with a window of 10 s. (**e**) As a comparison, a simple procedure to obtain estimates of elongation velocity is shown. First, ΔL outliers resulting from the algorithm (e.g. shown in green in panel (**a**)) are removed. Second, instantaneous elongation velocity is calculated from the trace of ΔL as a function of time. As can be observed, the error function fit to the kymograph provides better estimates of the position of the ends and displays less noise. Additionally, subtle changes in length at the pointed-end are detected which were not observed when using the length estimate from the automated filament tracing.

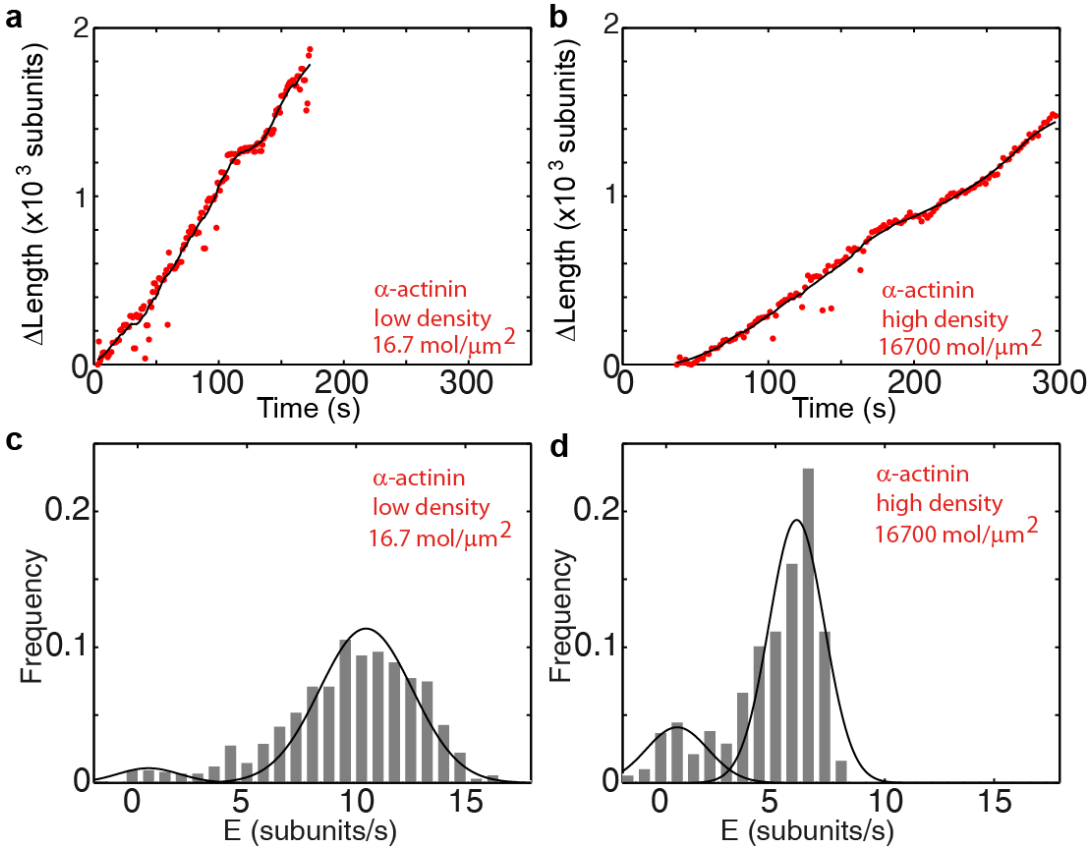

Figure S2. Actin filament elongation as a function of the surface density of α-actinin. a-b. The change in length, ΔL, as a function of time for a filament tether to the surface using α-actinin at surface densities of (**a**) low (16.7 molecules/μm^2) or (**b**) high density (16700 molecules/μm^2). **c-d**, The distribution of elongation velocities measured at (**c**) low or (**d**) high density. The histogram is calculated from the instantaneous elongation velocity, with a bin size is 0.75 sub/s, using more than 20 filaments. Solid lines are fits to Gaussian distributions.

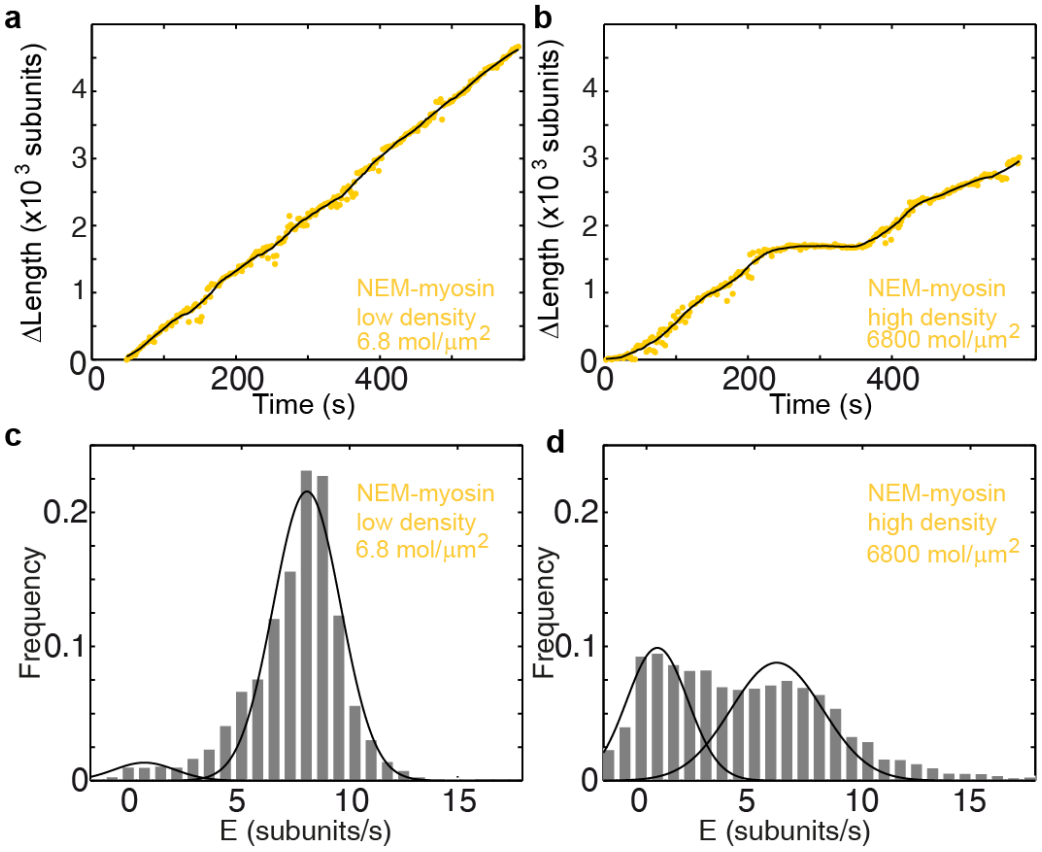

Figure S3. Actin filament elongation as a function of the surface density of NEM myosin. a-b. The change in length, ΔL, as a function of time for a filament tether to the surface using NEM-myosin at low (**a**) low (6.8 molecules/μm^2) or (**b**) high density (6800 molecules/μm^2).. **c-d**, Elongation velocity distribution of filaments using a NEM-myosin-coated surface at low (**c**) or high (**d**) density. The distribution is calculated by binning (0.75 sub/s bin size) the instantaneous elongation velocity of more than 20 filaments. Solid lines are fits to Gaussian distributions.

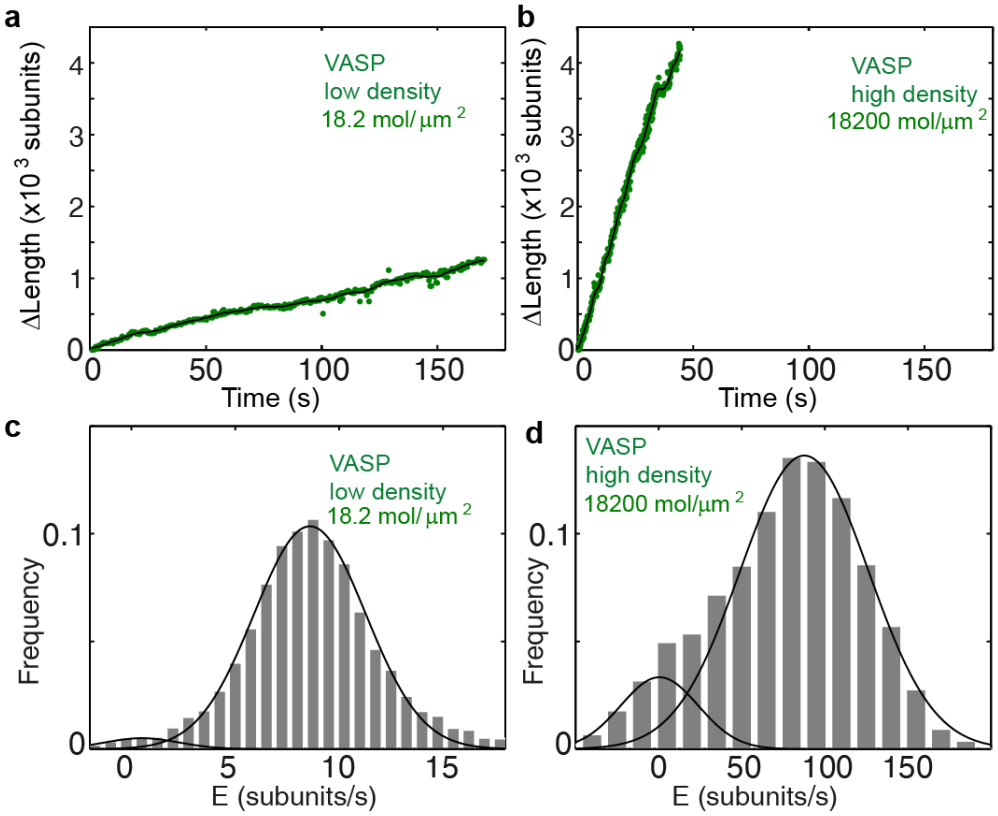

Figure S4. Actin filament elongation as a function of the surface density of VASP. a-b. The change in length, ΔL, as a function of time for a filament tether to the surface using VASP at low (**a**) low (18.2 molecules/μm^2) or (**b**) high density (18200 molecules/μm^2). **c-d**, Elongation velocity distribution of filaments using a VASP-coated surface at low (**c**) or high (**d**) density. The distribution is calculated by binning (0.75 sub/s and 10 sub/s bin size for low and high density, respectively) the instantaneous elongation velocity of more than 20 filaments. Solid lines are fits to Gaussian distributions.

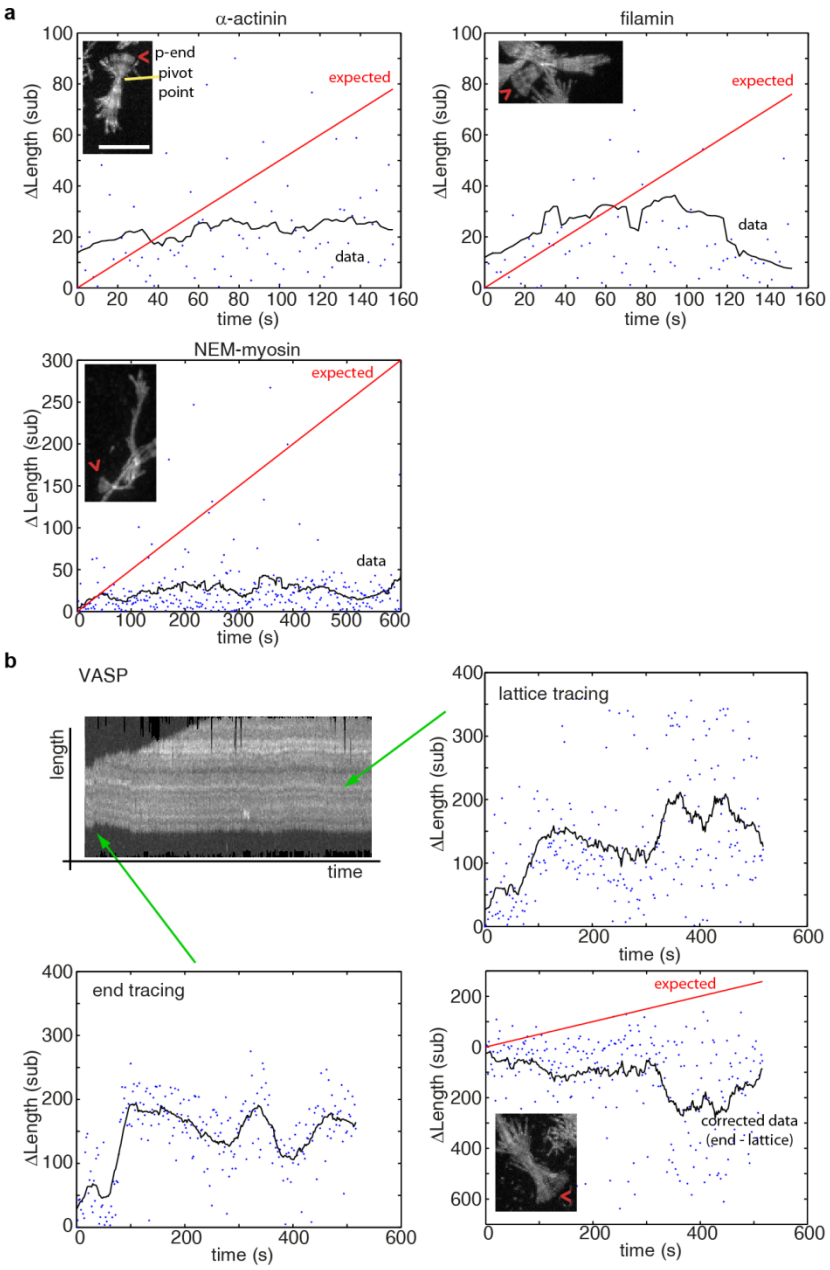

Figure S5. Pointed-end pausing on freely swiveling ends for various tethering proteins. a-b, The change in length of the pointed end of actin filaments as a function of time at 1 μM free actin concentration are shown when using (**a**) α-actinin, NEM-myosin, filamin and (**b**) VAPS as tethering proteins. Points represent raw data while black solid lines correspond to the data using a running mean with a window of 20 s. The solid red line is the elongation expected based on reported rates. A maximum projection image from the respective movie is shown as inset. **b**, (upper left panel) Kymograph of a growing filament showing lateral fluctuations due to weak binding of the filament to the tether. For accurate length determination with filament sliding, both

the pointed-end (lower left panel) and a fiduciary marker (upper right panel) were tracked. The corrected data (lower right panel) shows mostly a paused state. Data points here represent the position of the pointed end minus that of the fiduciary marker. Scale bar: 5 μm.

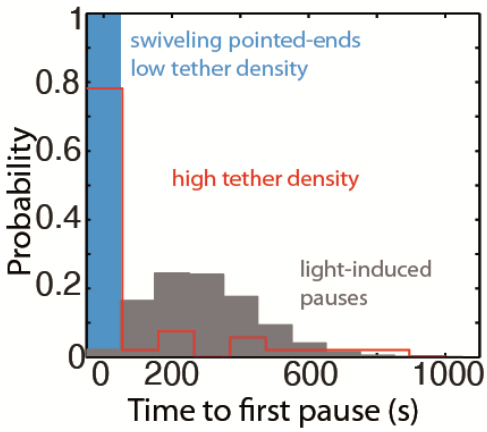

Figure S6. The distribution of the time to the first elongation pause at 300 nM free actin concentration. The distribution of the observed time to the first pause for depolymerizing pointed-ends at lowest tether density (blue bar) at medium to high tether density (pooled data, red bars); or predicted using a model for light induced dimerization (grey bars, see Materials and Methods).

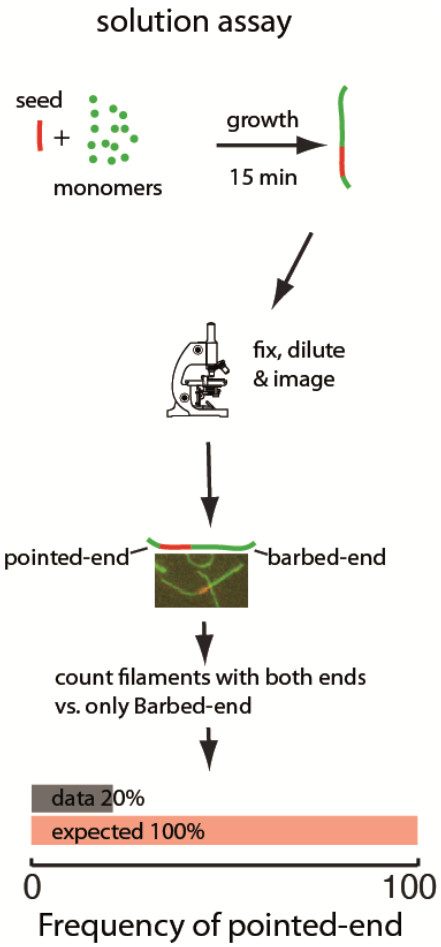

Figure S7. Two-color seeded assay for visualizing pointed-end growth from an actin filament seed. A schematic of the assay is shown. Actin filament fragments labeled in red with atto565 were used as seeds for filament growth in a solution of atto488-labeled (green) actin monomers. After 15 minutes, the reaction was stopped by addition of phalloidin and monomer dilution. Filaments formed during this time are therefore diluted and ease visualization of individual filaments. The filaments exhibiting growth at the barbed-end or at both ends were counted. The last figure shows the results of the analysis, were the observed (gray) and predicted (red) frequency of filaments with pointed-end growth are shown (n = 1000).

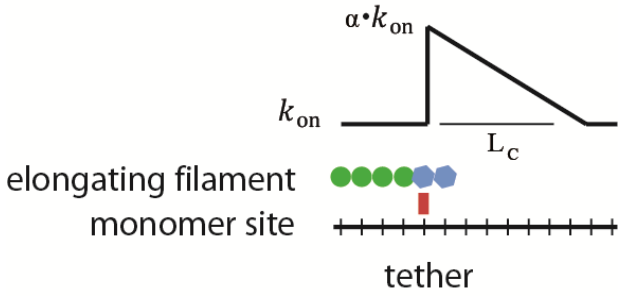

Figure S8. Schematic of the proposed model. Interaction of a lattice-binding protein (red square) with the actin filament (blue) alters the basal elongation rate (k_{on}^{0}) of successive association events by a factor α over a characteristic length L_C.

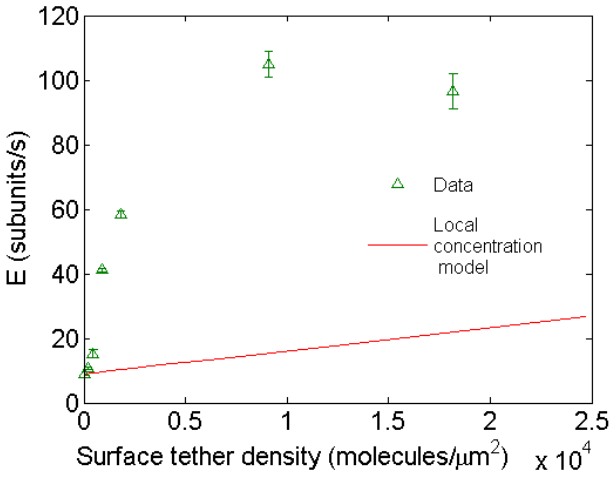

Figure S9. Comparison of the expected behavior using a higher local concentration mechanism with experimental results. Open green triangles are experimental data of barbed-end elongation as a function of VASP surface density in the presence of 1 μM free actin in solution. The solid line is the expected average E calculated with eq. 3 assuming a local increase in actin concentration due to the capacity of VASP to simultaneously bind four actin monomers.

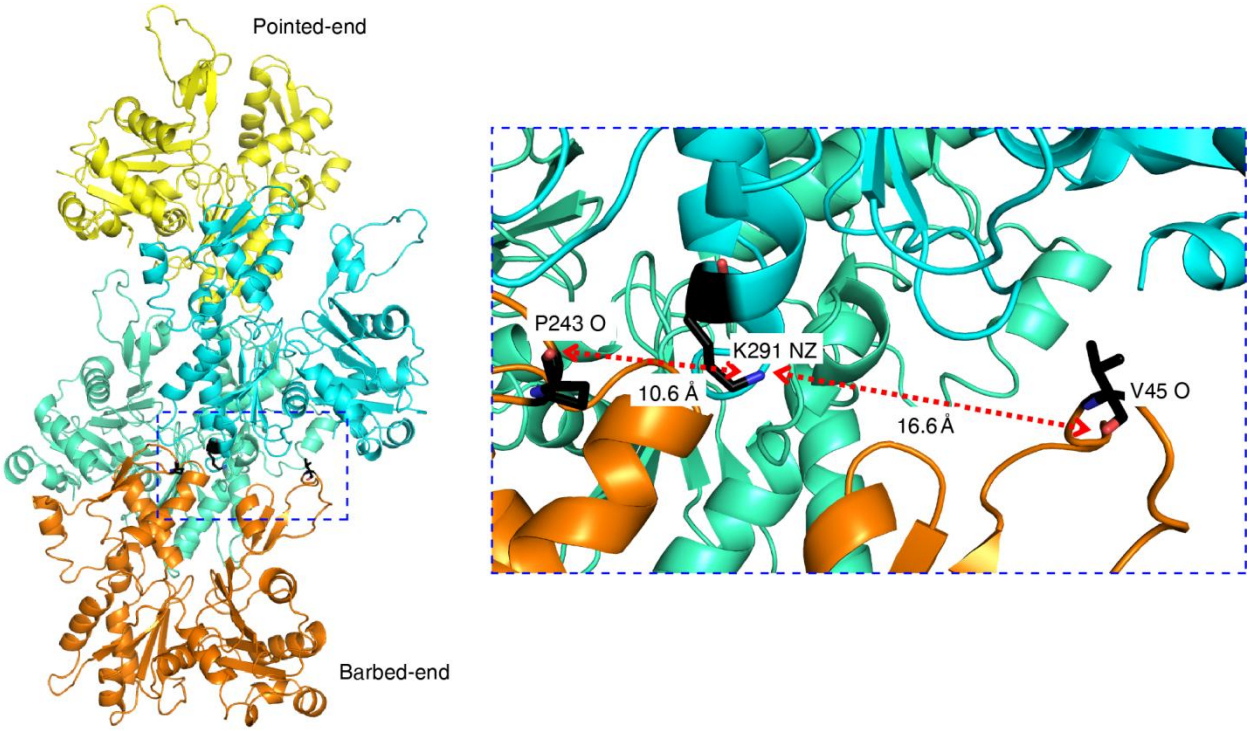

Figure S10. An example of an atom pair used previously as a reaction criterion for association and its comparison to our estimated values. For the pairs P243O-K291NZ and V45O-K291NZ, we measure 10.6 and 16.6 Å, respectively. The reported distances from (Sept et al., 1999) for these same pairs are 3.7 Å and 2.8 Å, respectively. Given our estimates, and the distance criteria of 3.5 Å or less for atom pairs defined for an association reaction, we do not use any of these atom pairs.

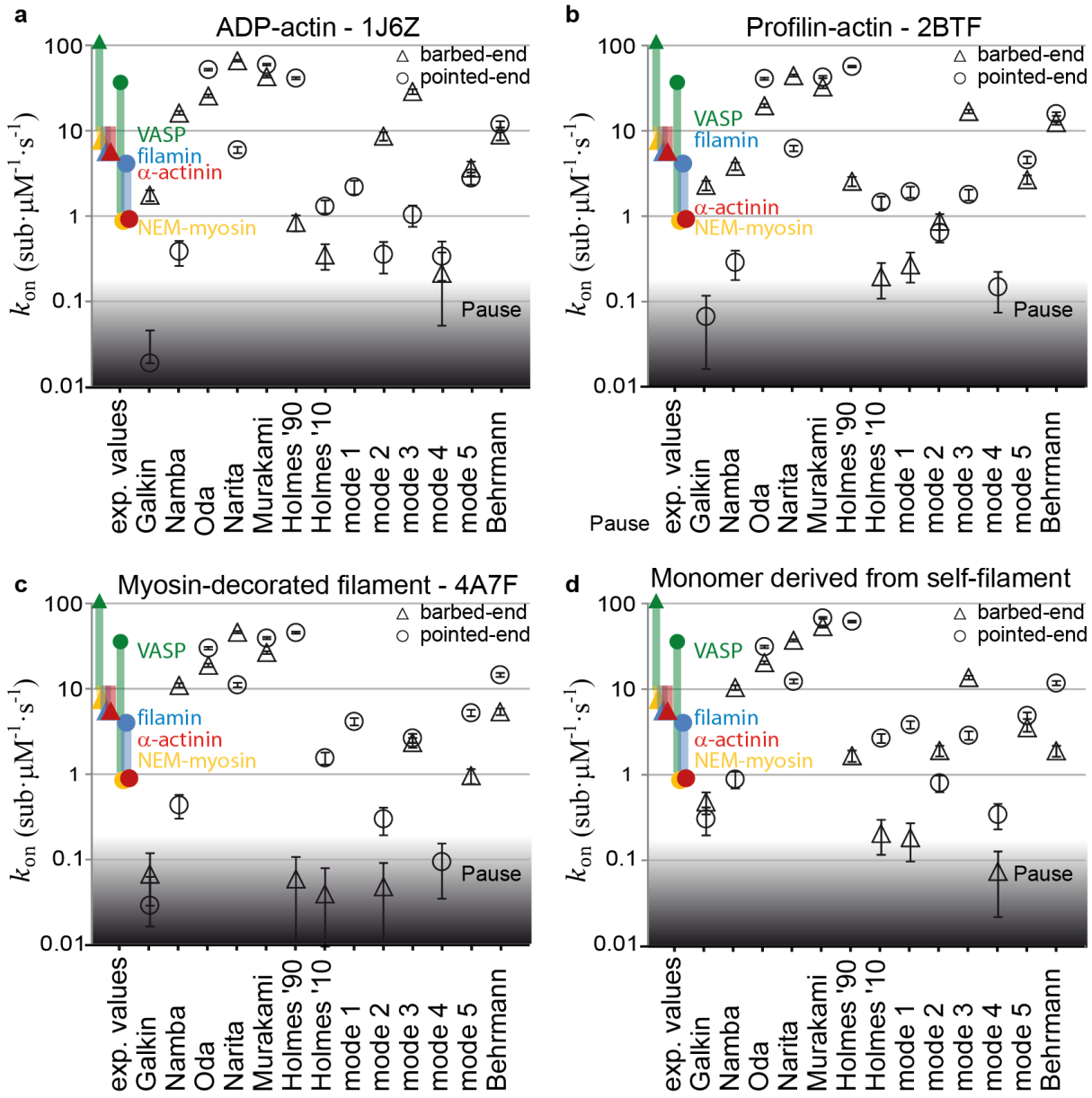

Figure S11. Association rates as a function of monomer and filament structures. a-d, Estimated barbed- (triangles) and pointed-end (circles) association rates via Brownian Dynamics simulations for the various filament models tests using the following structures for the monomer: (**a**) ADP-actin, (**b**) profilin-actin, (**c**) myosin-decorated filament and (**d**) a monomer derived from the same filament model. Only the actin and nucleotide molecule were used for calculations, i.e. additional proteins or small groups present in the crystal structure were removed. The grey shaded area represents values that would be observed as pauses in TIRF microscopy. Error bars represent the lower and upper estimate of the calculated rate.